Self-assembly of rigid magnetic rods consisting of single dipolar beads in two dimensions

Jorge L. C. Domingos,[1,2,*] François M. Peeters,[2] and W. P. Ferreira[1]
[1]*Departamento de Física, Universidade Federal do Ceará, Caixa Postal 6030, 60455-760 Fortaleza, Ceará, Brazil*
[2]*Department of Physics, University of Antwerp, Groenenborgerlaan 171, B-2020 Antwerpen, Belgium*
(Received 2 December 2016; published 17 July 2017)

Molecular dynamics simulations are used to investigate the structural properties of a two-dimensional ensemble of magnetic rods, which are modeled as aligned single dipolar beads. The obtained self-assembled configurations can be characterized as (1) clusters, (2) percolated, and (3) ordered structures, and their structural properties are investigated in detail. By increasing the aspect ratio of the magnetic rods, we show that the percolation transition is suppressed due to the reduced mobility of the rods in two dimensions. Such a behavior is opposite to the one observed in three dimensions. A magnetic bulk phase is found with local ferromagnetic order and an unusual nonmonotonic behavior of the nematic order is observed.

DOI: 10.1103/PhysRevE.96.012603

I. INTRODUCTION

Recent years has witnessed a growing interest in the self-assembly of magnetic nanoparticles (MNs) due to its wide range of applications, including magnetic fluids [1], biomedicine [2], magnetic resonance imaging (MRI) [3], data storage [4], magnetic filaments [5–7], among others. Basically, MNs are particles with a magnetic dipole moment, which are regarded as particles composed of a magnetic monodomain having a typical size from 15 to 150 nm [8]. Many efforts are currently being devoted to the synthesis and characterization of magnetic particles with anisotropic shape [9,10]. Within this area of research rodlike particles play an important role as active microrheology probes, because it is possible, by the torque provided by an uniform magnetic field, to enhance the visualization of their viscoelastic properties [11,12]. Other successful applications of magnetic rods are: (i) as components in micromechanical units [13–15], i.e., to generate localized particle trapping and stirring; (ii) as microscale propellers [16–18], i.e., magnetic units able to be remotely driven or guided in a fluid medium, and thus to potentially move and transport chemical or biological cargos in small channels or pores. Beyond the aforementioned applications, it has already been reported that particles with anisotropic shape show distinguished properties when compared to those of ferrofluids consisting of spherical particles, namely, magnetic birefringence [19] and thermal conductivity [20]. Recently, iron oxide nanorods were found to have potential for biomedical applications [21]. Colloidal rings and ribbons can be obtained from magnetic manipulation of Janus nanorods [22] and ferromagnetic ellipsoids [23].

In this work we present a numerical study of the self-assembly of a two-dimensional system of stiff magnetic rods, composed of single dipolar beads linked one by one through internal head-to-tail alignment. A similar system was used earlier in experiment [24] and simulations [25]. Our motivation to explore in more detail the two-dimensional (2D) situation is driven by the fact that many experiments involving assemblies of colloids are actually done at surfaces and/or thin films [26–30].

Our model is characterized by permanently linked dipolar beads so that the net interaction is given by the superposition of dipolar fields of single dipole beads. This opens the possibility of new kinds of assembled clusters distinct from rodlike particles with a *single* longitudinal (or transversal) dipole moment, which was intensively studied both by theory and simulations [31,32].

We also study the connectivity properties of the present system. The percolation behavior is of great relevance in highly connected materials due to the possibility of enhancing the electrical and thermal conductivity [24,33]. In general, percolation in polymers plays a fundamental role in properties related to conductivity, because in many cases percolation can be made responsible for electrical switching properties. A goal in studying the connectivity properties is to explore the conditions under which the percolation transition is enhanced. By using elongated particles, it was already shown that an increase of the aspect ratio decreases the percolation threshold [25,34]. The latter has also been realized by depletion effects [35] and by the application of an external field [25,36]. In the present work, we discuss the connectivity properties of magnetic rods in a 2D system, and show that the percolation transition with respect to the density behaves opposite as compared to the 3D case.

The last aim of this study is to analyze the appearance of orientational ordering. It is already known that elongated particles present nematic and smetic transitions driven by entropic effects so that they are isotropic for low densities and nematic for high densities [37]. In a recent study of a 3D system of magnetic nanorods (MNR), similar to the ones studied in this work, an improvement of the stability of the nematic phase was found for sufficiently long MNRs as a consequence of the interaction resulting from the arrangement of the dipoles along each MNR [25]. In our 2D system we find a different scenario, where a nonmonotonic behavior of the nematic order parameter is observed for sufficiently long MNRs, as a consequence of the appearance of magnetic bulk domains.

The paper is organized as follows: our model system is presented in Sec. II. The results for the different cluster configurations are presented in Sec. III. The connectivity properties are discussed in Sec. IV and the ordered configurations in Sec. V. Our conclusions are given in Sec. VI.

*jorgecapuan@fisica.ufc.br

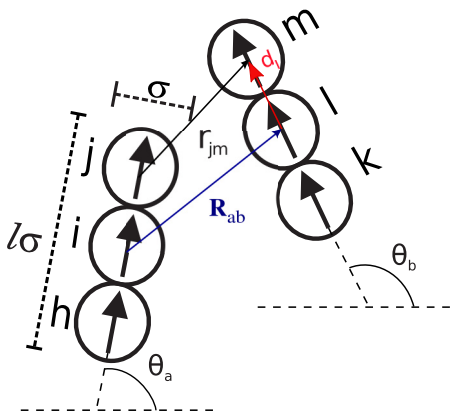

FIG. 1. Schematic illustration of the interaction between two magnetic rods with indication of the important parameters of the pair interaction potential.

II. MODEL

Molecular dynamics (MD) simulations were used to investigate two-dimensional (2D) systems consisting of 2520 up to 2820 identical soft beads of diameter σ with a pointlike magnetic dipole at their center. A stiff rod is formed by those soft beads, with their positions fixed with respect to the center of mass of the rod. The orientation of the dipoles is always aligned along the rod, as illustrated in Fig 1. The length of the rod is defined as $l\sigma$, where l is the number of beads, which is also its aspect ratio. To model the dipolar particles we use a dipolar soft sphere (DSS) potential [38], consisting of the repulsive part of the Lennard-Jones potential $u^{\rm rep}$ and a pointlike dipole-dipole interaction part u^D. It was found that this potential does not induce a vapor-liquid phase transition as, e.g., the Stockmayer potential does [38,39]. The interaction energy between two rods a and b is the sum of the pair interactions between their respective dipolar spheres (DS):

$$U_{a,b}(\mathbf{R}_{a,b},\theta_a,\theta_b) = \sum_{j\neq m} u_{j,m}, \tag{1}$$

$$u_{j,m} = u^{\rm rep}\left(\mathbf{r}_{jm}^{a,b}\right) + u^{D}\left(\mathbf{r}_{jm}^{a,b},\boldsymbol{\mu}_j^a,\boldsymbol{\mu}_m^b\right), \tag{2}$$

where

$$u^{\rm rep} = 4\epsilon\left(\frac{\sigma}{r_{jm}}\right)^{12}, \tag{3}$$

$$u^{D} = \frac{\boldsymbol{\mu}_j\cdot\boldsymbol{\mu}_m}{r_{jm}^3} - \frac{3(\boldsymbol{\mu}_j\cdot\mathbf{r}_{jm})(\boldsymbol{\mu}_m\cdot\mathbf{r}_{jm})}{r_{jm}^5}, \tag{4}$$

with $\mathbf{R}_{a,b}$ the vector joining the center of rods a and b with orientations θ_a and θ_b. The vector $\mathbf{r}_{jm}^{a,b}$ connects the center of bead m of rod a with respect to the center of bead j of rod b (Fig. 1). The force between two beads is given by

$$\mathbf{f}_{jm} = -\nabla u_{jm}. \tag{5}$$

The torque on bead m (see the Appendix) is

$$\mathbf{N}_m = \boldsymbol{\mu}_m \times \sum_{m\neq j}\mathbf{B}_{jm} + \mathbf{d}_m \times \sum_{m\neq j}\mathbf{f}_{jm}, \tag{6}$$

where $\mathbf{d}_m$ is the vector joining the center of the rod with the center of bead m, as illustrated in Fig. 1 and $\mathbf{B}_{jm}$ is the magnetic field generated by the dipole moment μ_j at the position of the dipole μ_m, which is given by

$$\mathbf{B}_{jm} = \frac{3(\boldsymbol{\mu}_m\cdot\mathbf{r}_{jm})\mathbf{r}_{jm}}{r_{jm}^5} - \frac{\boldsymbol{\mu}_m}{r_{jm}^3}. \tag{7}$$

The summations in Eq. (6) are considered only for dipoles belonging to distinct rods. The orientation of the rods is given by a unitary vector $\mathbf{s}$ given by $\mathbf{s} = \mathbf{d}_m/\mid\mathbf{d}_m\mid$. We solve the translational and rotational equations of motion using a leapfrog algorithm:

$$r_\alpha(t+\delta t) = r_\alpha(t) + v_\alpha(t+\delta t/2)\delta t, \tag{8}$$

$$s_\alpha(t+\delta t) = s_\alpha(t) + u_\alpha(t+\delta t/2)\delta t. \tag{9}$$

The subindex α refers to the α component of the vectors $\mathbf{r}$, $\mathbf{v}$, $\mathbf{s}$, and $\mathbf{u}$, with $\mathbf{u} = \boldsymbol{\omega}\times\mathbf{s}$, where ω is the angular velocity. We introduce the reduced units $t^* = t/\sqrt{\epsilon^{-1}m\sigma^2}$ for time, where m is the mass of the rod, $U^* = U/k_BT$ is for energy, where k_B is the Boltzmann constant, $\mu^* = \mu/\sqrt{k_BT\sigma^3}$ is for dipole moment, and, finally, $r^* = r/\sigma$ is for position. The ratio of thermal energy to soft-sphere repulsion constant is chosen as $k_BT/\epsilon = 0.1$, which is also our reduced unit of temperature $T^* = Tk_B/\epsilon$. In order to fix the temperature, we employ the Berendsen thermostat [40–42] with a time constant $\tau = 2\delta t$, where the time step was taken as $\delta t = 0.005$–0.01. Periodic boundary conditions are taken in both spatial directions. In the 2D case, the dipolar pair interaction falls off fast (r^{-3}) and therefore it is sufficient to take the simulation box sufficiently large such that no special long-range summation techniques [43] has to be used as in the case for, e.g., Coulomb $1/r$ interactions. We define the packing fraction as $\eta = \rho^* l\pi/4$, where ρ^* is the dimensionless density $\rho^* = \rho\sigma^2$.

To check the equilibration in our simulations we follow the total energy as a function of time. In equilibrium, the total energy fluctuates around an average value. For very dilute systems ($\eta < 0.2$) the equilibrium is reached after 1×10^6 time steps ($1\times10^4\sqrt{\epsilon^{-1}m\sigma^2}$), while for $\eta \geqslant 0.2$ we need about 5×10^5–1×10^6 time steps ($2.5\times10^3\sqrt{\epsilon^{-1}m\sigma^2}$–$5\times10^3\sqrt{\epsilon^{-1}m\sigma^2}$). Time averages over energies and other quantities are taken over 1×10^6 time steps after equilibrium is reached. Unless stated, we consider $\sigma^* = 1$ and $\mu^{*2} = 10$, which means that each bead has the same magnitude of dipole moment. Such a value is justified by the fact that we aim to investigate the weak coupling regime, in order to emphasize the geometrical effects due to the increase of the aspect ratio of the particles. Common experimental values of μ^{*2} at room temperature ranges in the interval $1 \leqslant \mu^{*2} \leqslant 100$. For example, in experiments using iron nanoparticles [24], it is found that the saturation magnetization $M_s(\mathrm{Fe}) = 1700\,\mathrm{kA/m}$ and the radius of the particles is $r \approx 5$ nm. In this case, we estimate $\mu^* \approx 4.4$ at room temperature ($T \approx 293$ K). Also, in experiments [44] carried out using aqueous dispersions of superparamagnetic microspheres of ferrite grains [Estapor (R) from Merck—reference M1-030/40] for $r \approx 205$ nm and $M_s \approx 6\times10^4$ A/m, the magnetization (M) of the particles is completely reversible and adjustable by an external magnetic

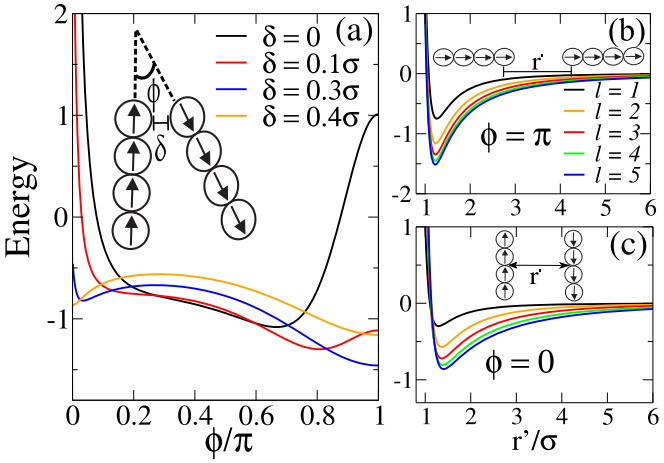

FIG. 2. The pair interaction energy (a) as a function of the angle ϕ for different inter-rod separation δ, (b) as a function of the interparticle distance for $\phi = \pi$, and (c) for $\phi = 0$. In (b) and (c) the different colors represent different values of the aspect ratio, indicated in (b).

field. If we consider $T = 293$ K and $M \approx 22.6\%$ of M_s on that system, we obtain $\mu^* \approx 3.16$ ($\sim \sqrt{10}$).

The minimum energy configuration was chosen among the ones obtained by running simulations several times (10–30), each with distinct initial conditions (coordinates and momenta).

III. CLUSTER FORMATION

We start by presenting the dependence of the DSS pair interaction potential on the angle and separation between the rods. The study of the pair interaction potential is interesting to understand the nature of the resulting many-body interaction and to help us to set the values of the parameters useful to analyze the results. The dependence of the DSS pair interaction potential as a function of the angle ϕ between rods (with aspect ratio $l = 4$) is presented in Fig. 2(a) for different separation δ. The separation δ is defined as the shortest distance between two rods for a given angle [see inset in Fig. 2(a)]. We choose $\delta = 0.4\sigma$ as the separation distance at which we consider two rods as being bonded. In Fig. 2(a) the curve for $\delta = 0.4\sigma$ exhibits a local minimum for $\phi = 0$ and a global minimum at $\phi = \pi$, justifying our choice for the critical value of δ. The results shown in Fig. 2 are for $l = 4$, but the same critical distance was taken for all values of l considered in this study, since such a behavior of the interaction potential remains for different l values. The dependence of the pair interaction potential with respect to the separation between two rods for different aspect ratio is shown in Fig. 2(b) for $\phi = \pi$ (parallel head-to-tail alignment) and in Fig. 2(c) for $\phi = 0$ (side-by-side dipoles with opposite orientation). In both cases, the attraction for low separation increases with increasing aspect ratio. Note that the parallel head-to-tail assembly ($\phi = \pi$) is energetically more favorable for the formation of chains, for every l, as found in ferrofluids in the absence of external magnetic fields, both in simulations [45–47] and in experiment [48].

The attraction between magnetic rods becomes stronger for larger l, suggesting that, in the many-body case, the formation of clusters is facilitated as l increases. To show this is indeed the case, we analyze the degree of polymerization [49], defined as

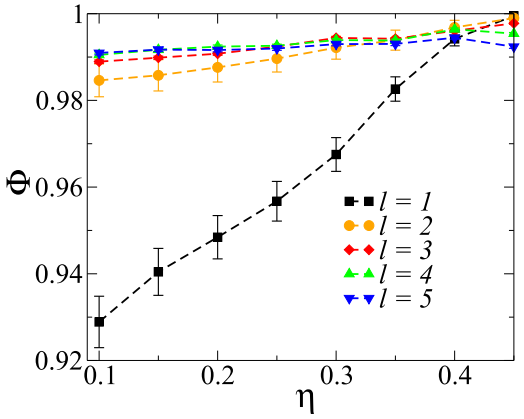

FIG. 3. The polymerization as a function of the packing fraction η for different aspect ratios.

$$\Phi = \left\langle \frac{N_c}{N} \right\rangle, \tag{10}$$

where N_c is the number of clustered rods and N is the total number of rods.

In Fig. 3 the polymerization Φ as a function of η is presented for a different aspect ratio. In general $0.92 < \Phi < 1$, which is consistent with a previous molecular dynamics study of dipolelike colloids [50] for $T^* = 0.1$, where Φ increases with increasing η. For $l = 1$, the behavior stands out from the other l values, which is a consequence of the increase of the interparticle attraction with increasing l for low packing fraction as shown in Figs. 2(b) and 2(c). For $\eta \geqslant 0.4$, the degree of polymerization presents the opposite dependence with respect to l, i.e., Φ decreases with increasing l. Since in highly dense systems, the larger aspect ratio of the rods introduces strong depletion interaction restricting the head-to-tail arrangements of the rods. We discuss such a behavior in more detail in the next section.

Some representative equilibrium configurations are presented in Fig. 4. The head-to-tail tendency is present in all configurations. For low packing fraction the chains can form rings, which are not observed for $l = 5$ due to geometrical reasons. In the large packing fraction regime ($\eta \geqslant 0.4$) the side-by-side arrangement comes into play.

We analyze the structure of the system by computing the pair correlation function [51]:

$$\mathbf{g(r)} = \frac{\left\langle \sum_a \sum_{b \neq a}^{N} \delta(r - R_{ab}) \right\rangle}{2N\pi r \rho^*}, \tag{11}$$

where R_{ab} is the separation between the center of the rods a and b (see Fig. 1). As shown in Fig. 5(a), for low packing fraction, the position of the multiple peaks are related to the length of the rod for all l. This is the result of the head-to-tail alignment of neighboring rods. For a higher packing fraction ($\eta = 0.4$) intermediate peaks are observed [Fig. 5(b)]. For example, for $l = 3$, besides peaks at multiples of 3σ, there is a peak at $r \approx 1.8\sigma$. For $l = 5$, there are peaks at $r \approx 1.8\sigma$ and $r \approx 3.8\sigma$. These intermediate peaks are due to the side-by-side

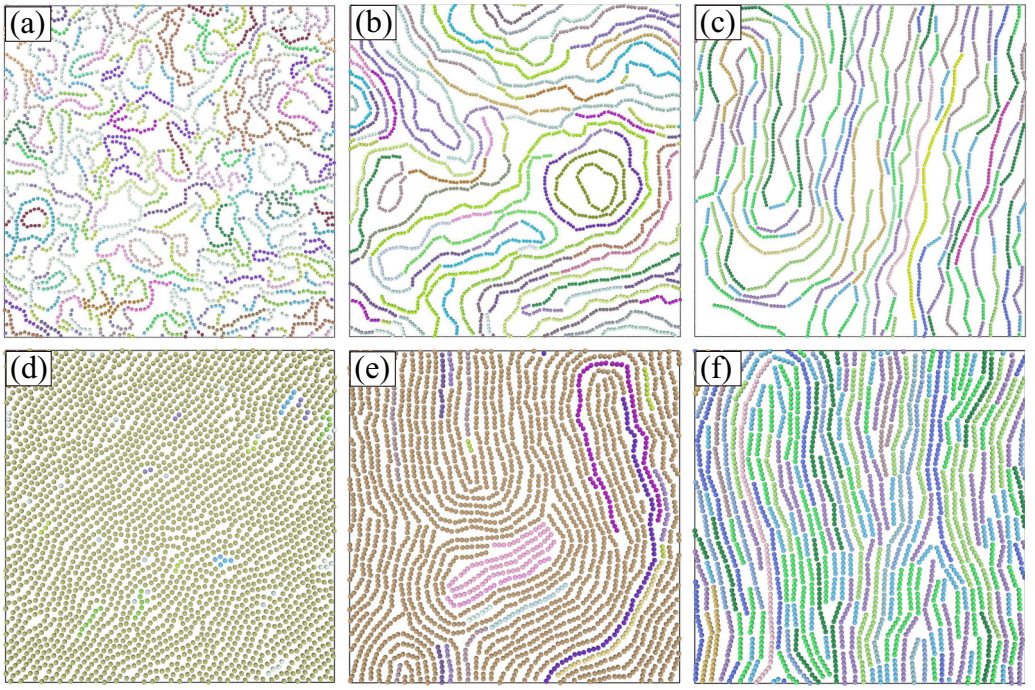

FIG. 4. Some representative equilibrium configurations for $T^* = 0.1$. Each color represents a different size of cluster. (d) and (e) Percolated systems. (a) $\eta = 0.2$, $l = 1$; (b) $\eta = 0.2$, $l = 3$; (c) $\eta = 0.2$, $l = 5$; (d) $\eta = 0.4$, $l = 1$; (e) $\eta = 0.4$, $l = 3$; (f) $\eta = 0.4$, $l = 5$.

configuration of neighboring rods, either parallel, antiparallel, or both.

In order to better understand the microstructure of the clusters, we calculate the angle correlation $f(\theta)$ among the first neighboring rods, defined as

$$f(\theta) = \frac{1}{A}\left\langle \sum_{a}\sum_{b\neq a}^{N} \delta(\theta - \theta_{ab}) \right\rangle \quad \text{for} \quad r_{ij} \leqslant \delta_c, \qquad (12)$$

where $\theta_{ab} = \theta_a - \theta_b$ (see Fig. 1), $r_{ij} = |\mathbf{r}_i - \mathbf{r}_j|$ is the separation between dipole i and dipole j, and A is the normalization constant, defined as $A = \int_0^{\pi} f(\theta) d\theta$.

The function $f(\theta)$, Eq. (12), calculated for rods with distinct lengths and for different packing fractions is presented in Fig. 6. The rods are mostly connected to each other along the same direction, i.e., $f(\theta)$ is more pronounced around $\theta/\pi = 0$ and $\theta/\pi = 1$. The former trend reflects the head-to-tail or the parallel alignment, while the latter trend is related to the antiparallel arrangement. The larger the packing fraction the larger $f(\theta)$ is around $\theta/\pi = 1$. The angle correlation for $\theta = \pi$ as a function of the packing fraction η is shown in the inset of Fig. 6. As expected, the frequency of antiparalell arrangement increases with increasing η. The η dependence of $f(\theta)$ is qualitatively the same for distinct aspect ratios. The case $\theta = 0$ was not considered in the insets because it represents two kinds

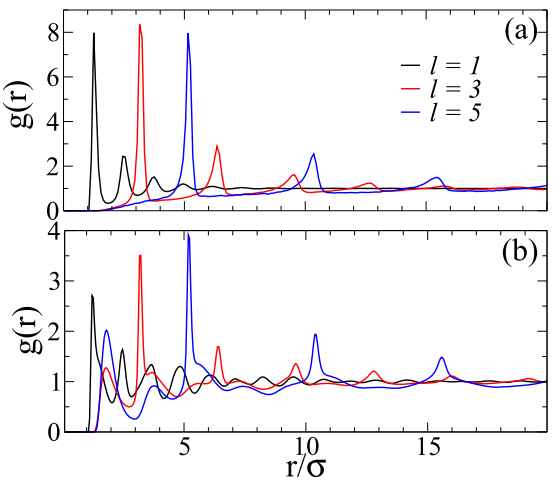

FIG. 5. The pair correlation function for different aspect ratio and for (a) $\eta = 0.1$ and (b) $\eta = 0.4$.

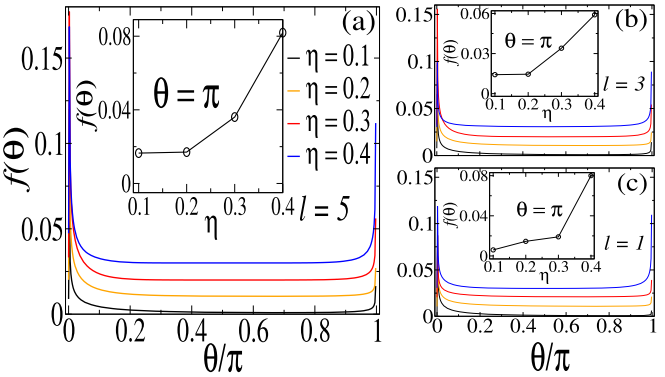

FIG. 6. The angle correlation between the nearest neighboring particles for (a) $l = 5$, (b) $l = 3$, (c) $l = 1$; and different values of η. Subsequent curves are shifted by 0.01 along the y axis in order to accentuate the small differences. The angle correlation for $\theta = \pi$ as a function of the packing fraction η is presented in the inset of each figure.

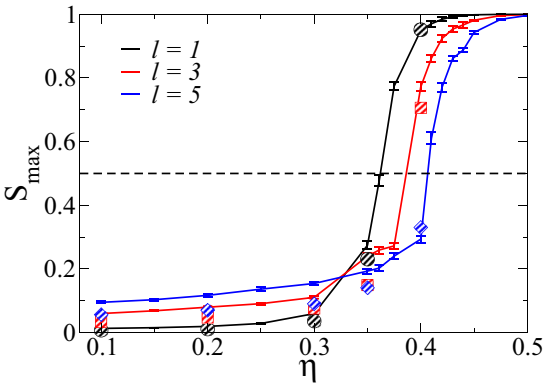

FIG. 7. The average fraction of monomers in the largest cluster that is present in the ground state configuration as a function of packing fraction for a different aspect ratio. The horizontal dashed line at 0.5 represents the percolation threshold. The results of the simulation for twice the number of particles in the computational unit cell is represented by symbols.

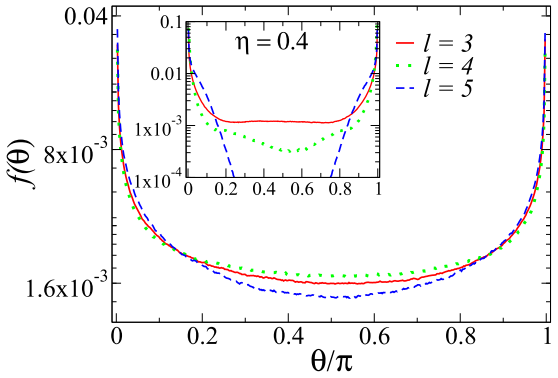

FIG. 8. The angle correlation between the nearest neighboring rods excluding the parallel head-to-tail alignment for $\eta = 0.1$. Results for $\eta = 0.4$ are shown in the inset. In both cases the y axis is in log scale.

of arrangements, the parallel side-by-side and the parallel head-to-tail. In the next section, the side-by-side arrangement is discussed in more detail.

IV. CONNECTIVITY PROPERTIES

In this section we examine the connectivity properties of the self-assembled structures by studying the percolation transition, which is marked by the formation of an infinite cluster spanning over the system. Configurations are percolated when, accounting for periodic boundary conditions, one of the cluster forms a percolating path [52], i.e., the cluster is connected through the opposite borders of the simulation box. For systems with transient bonds the percolation transition is defined in the thermodynamic limit, where the average cluster size diverges [53]. For systems with a finite size of computational unit cell, the fraction of monomers in the largest cluster $S_{\max}$ can be taken as the order parameter [54,55], namely

$$S_{\max} = \left\langle \frac{N_{\text{larg}}}{N} \right\rangle, \tag{13}$$

where N_{larg} is the number of rods belonging to the largest cluster. For finite size systems, the percolation transition is well characterized when $S_{\max} = 0.5$ [55]. Here we evaluate $S_{\max}$ as a function of the packing fraction. Such an order parameter was considered in the study of the gelation transition [54,56], which is related to the connectivity properties of the system. It has already been reported that 3D systems with elongated particles exhibit a percolation transition for lower density when their aspect ratio increases [25,34].

In Fig. 7 we show the average size of the largest cluster ($S_{\max}$) as a function of the packing fraction for $l = 1$, $l = 3$, and $l = 5$. $S_{\max}$ can be interpreted as the probability that one monomer belongs to the largest cluster. Notice that the percolation transition is shifted to larger packing fraction with increasing l, which is opposite to what is found in 3D systems of elongated magnetic rods [25].

In order to better understand these results, we show in Fig. 8 the angle correlation [see Eq. (12)] excluding the parallel head-to-tail alignment, so that $\theta = 0$ ($\theta = \pi$) means parallel (antiparallel) arrangement of the bonded side-by-side rods. For low packing fraction ($\eta = 0.1$), a large diversity of possible alignments beyond the side-by-side arrangements are found [e.g., see also Fig. 4(b)]. However, a higher probability for side-by-side arrangement is found for larger η and larger l. For $l = 5$, the possible nonhead-to-tail arrangements are mainly side-by-side arrangements, either parallel or antiparallel (see inset of Fig. 8).

Note from Figs. 2(b) and 2(c) that the attractive well is wider and shallower in the antiparallel case [see Fig. 2(c)], which allows thermal fluctuations to break the clusters more easily, and make the largest cluster more unstable. In addition, the larger the aspect ratio, the harder it is for the rods to form large clusters in a head-to-tail arrangement. Since the percolated cluster is essentially characterized by head-to-tail bonds, such a condition is more difficult to realize for large l. As a consequence, the percolation transition is shifted to larger η when l increases. Although not shown, we find that the head-to-tail arrangement is also more stable than a parallel side-by-side arrangement.

Clusters that extend across the computational unit cell appear in Figs. 4(d) and 4(e). Note that the largest cluster almost extends over the whole system. In the head-to-tail alignment, the rods form chains, which are, in some cases, curved or circular paths.

Now we study the dependence of the cluster size distribution $n(s)$ on the aspect ratio of the magnetic rods. In Fig. 9 we present the average cluster size distribution for $\eta = 0.4$. In general, $n(s)$ decreases with increasing cluster size. Close to percolation $n(s)$ develops a power-law dependence with exponent $\tau \approx -2.05$, which is related to the random percolation prediction made for a 2D system ($\tau = -187/91 = -2.055$) [57] in the thermodynamic limit. Due to the finite size of the system considered in the simulations, percolated fluids exhibit a single peak for large s, comparable to the system size, and these states are denoted as random percolated [58,59]. The $n(s)$ curves also confirm that the percolation transition for the system with larger aspect ratio takes place

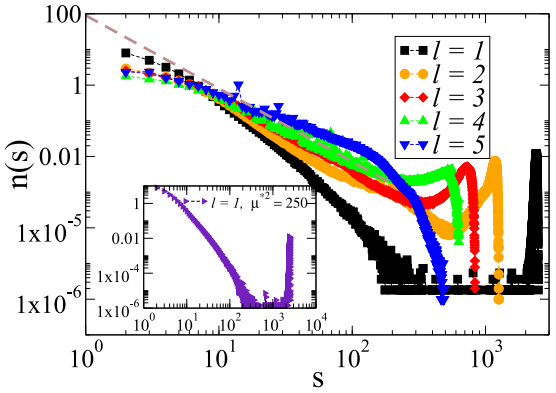

FIG. 9. The cluster size distribution for $\eta = 0.4$, and different aspect ratios. The dashed line represents the function $n(s) \approx s^{-2.05}$. In the inset, the $l = 1$ case for $\mu^{*2} = 250$. Both axes are in log scale.

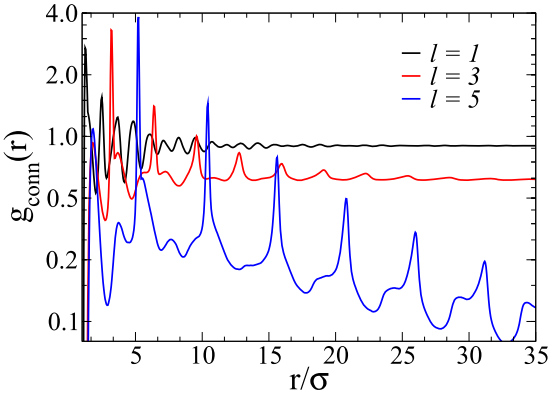

FIG. 10. The pair connectedness function for different aspect ratio values for packing fraction $\eta = 0.4$. The y axis is in log scale.

for larger η. The increase of the aspect ratio of the rods results in a stronger interaction between rods due to the addition of soft beads. Note that the case with $l = 5$ and $\mu^{*2} = 10$ is not percolated, while for $l = 1$ and $\mu^{*2} = 10$ it is percolated (Fig. 9). Each bead contributes with $\mu^* = \sqrt{10}$, to the net dipole moment of the rod, in order that for $l = 5$ the net dipole moment is $\mu^*_{\text{net}} = 5\sqrt{10}$ or $\mu^{*2}_{\text{net}} = 250$. With these numbers ($l = 1$, $\mu^* = 10$ percolated, and $l = 5$, $\mu^* = 250$ not percolated) it is not clear whether the stronger interaction or the larger aspect ratio of the rods (or both effects) is relevant to prevent the formation of the percolated configuration. To check the importance of the interaction between rods in driving the percolation transition, we study the case in which the rods have aspect ratio $l = 1$ and $\mu^{*2} = 250$, for packing fraction $\eta = 0.4$, which is shown as an inset in Fig. 9.

Our findings indicate that, although the dipolar nature of the interaction is fundamental to the results found in the present study, since the percolation threshold for noninteracting rigid rods in a two-dimensional system decreases with increasing aspect ratio [60,61], the geometric effect (aspect ratio and 2D confinement) is the determining factor that rules the connectivity behavior of the system. Another useful quantity to obtain information about percolation is the pair connectedness function $g_{\text{conn}}(r)$, which is defined as the conditional probability of finding a particle at a distance r from a particle located at the origin, connected via a sequence of bonds, i.e., within the same cluster [62]. In the limit when the whole system forms a single cluster, the pair connectedness function matches the pair correlation function [Eq. (11)].

In Fig. 10 we show $g_{\text{conn}}(r)$ for different aspect ratios and for packing fraction $\eta = 0.4$. For an infinite-size cluster, $g_{\text{conn}}(r)$ becomes different from zero in the limit $r \to \infty$. From what is presented in Figs. 7 and 9, percolation is suppressed when we increase the aspect ratio of the rods, so that for packing fraction $\eta = 0.4$ the $l = 1$ and $l = 3$ cases are percolated, while on the other hand, the $l = 5$ case is not. We see that such a behavior is also clearly reflected in $g_{\text{conn}}(r)$. The results presented in this section indicates that the dependence of the percolation transition on the packing fraction is mainly ruled by geometric effects.

V. ORIENTATIONAL ORDERING

In this section we investigate the appearance of orientational order. 3D suspensions of passive rodlike particles in thermal equilibrium were found to be isotropic for low densities and nematic for high densities [37]. Here we investigate the occurrence of liquid-crystalline ordering in 2D by analyzing the ferromagnetic order parameter G_1, i.e., the polarization

$$G_1 = \left\langle \frac{1}{N} \left| \sum_i^N \hat{\boldsymbol{\mu}} \cdot \hat{\boldsymbol{d}} \right| \right\rangle, \tag{14}$$

where N is the number of rods, $\hat{\boldsymbol{\mu}} = \boldsymbol{\mu}/|\boldsymbol{\mu}|$, and $\hat{\boldsymbol{d}}$ is the unit eigenvector related to the largest eigenvalue (G_2) of the following matrix:

$$\boldsymbol{Q}_{kf} = \frac{1}{2N} \sum_i^N \left(3\hat{\boldsymbol{\mu}}^i_k \hat{\boldsymbol{\mu}}^i_f - \delta_{kf}\right), \tag{15}$$

where i refers to particle i and the indexes k and f denote the cartesian components of the orientation vector. G_2 is also referred to as the orientational order parameter, i.e., the nematic order parameter [43]. As shown in Fig. 11(a), the polarization is negligible for any l, indicating that no ferromagnetic ordering is present. On the other hand, Fig. 11(b) indicates that an orientational order of the rod axes is present. As expected, an increase of the aspect ratio shifts the increase of G_2 towards lower packing fraction. In the case of a single dipole ($l = 1$) we observe a rather distinct isotropic-nematic transition as compared to the $l \neq 1$ cases. These results are consistent with the findings of Alvarez *et al.* [25], in the sense that a larger aspect ratio increases the stability of the nematic phase. However, we also find a nonmonotonic behavior of the orientational ordering for high packing fraction due to the presence of magnetic bulk domains, which present local ferromagnetic order. Monte Carlo simulations of a corresponding 2D systems revealed frustrated structures characterized by large domains of local ferroelectric order, but no long-range order [63], which are consistent with the present study. In a 2D system at finite temperature, the nematic and smetic transition is not observed for long-range interaction [64–67]. On the other hand, the magnetic dipolar interaction in 2D is short range, in order that it is possible to observe such an isotropic-nematic

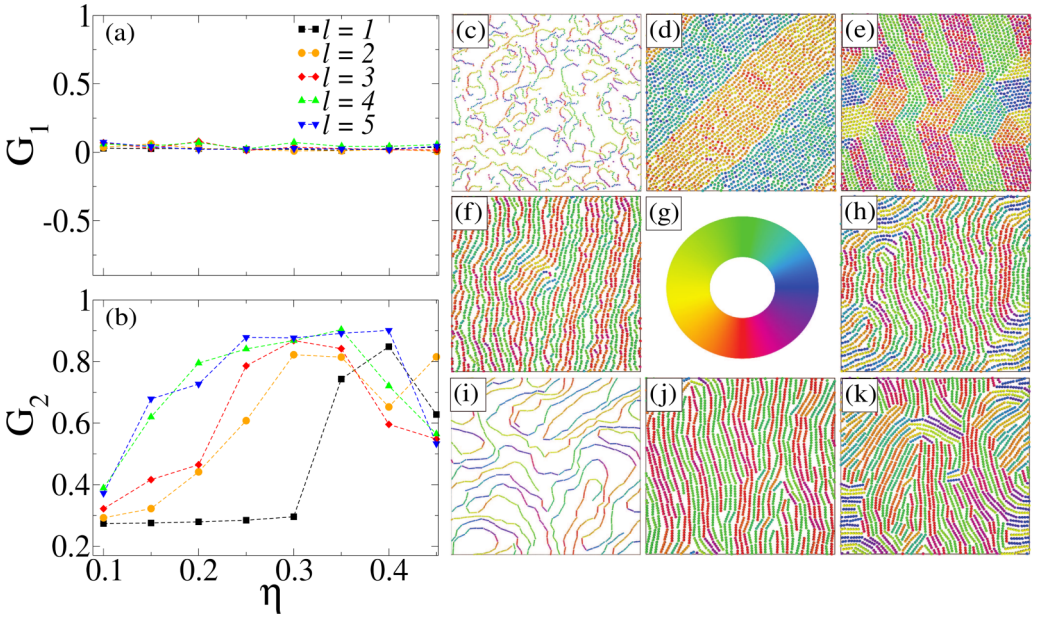

FIG. 11. (a) The polarization and (b) the nematic order parameter for different aspect ratios as a function of the packing fraction. The orientation of some representative configurations are depicted in the right figures for $T^* = 0.1$ and for $l = 1$ with (c) $\eta = 0.1$, (d) $\eta = 0.4$, (e) $\eta = 0.45$ and for $l = 2$ with (f) $\eta = 0.4$, (h) $\eta = 0.45$ and for $l = 5$ with (i) $\eta = 0.1$, (j) $\eta = 0.4$; (k) $\eta = 0.45$. (g) The colors indicate the orientation of the dipoles in plane.

transition [68,69]. In Figs. 11(c)–11(k) it is possible to observe the orientation of the rods for different configurations. In Fig. 11(e) a local hexagonal order can be seen as a consequence of the fact that for low temperature and sufficiently high density the dipolelike colloids form crystalline structures (positional ordering). Such a local-hexagonal order of the corresponding 2D system at $T^* = 0.1$ was recently reported by Schmidle *et al.* [50]. An interesting lanelike configuration is shown in Fig. 11(d). Previously, a similar lane formation for a binary mixture of particles driven against each other by an external field was predicted [70,71]. The lane formation is an instability where, for strong enough driving forces, alike particles are driven to move behind each other in order to avoid collisions with oppositely driven particles. A similar structure was also reported for self-propelled particles [68,72,73]. In the present study, the lane formation appears in a monodispersive system as a nematic and an intermediate isotropic-hexagonal ordering transition of circular ($l = 1$) particles provided by the magnetic interaction, which makes particles in the different lanes distinct due to the opposite orientation of their dipoles.

VI. CONCLUSIONS

In summary, we investigated a two-dimensional system consisting of magnetic rods using molecular dynamics simulations. Each rod was composed of soft beads having a central pointlike dipole which interact via a DSS potential. This model was motivated by recent experimental [24] and theoretical [25] studies. Structural properties were investigated with particular attention to the dependence on the aspect ratio and the packing fraction. We considered aspect ratios ranging from $l = 1$ to $l = 5$.

The head-to-tail assembly was identified as the most energetically favorable for any aspect ratio. Such a configuration favors the formation of chain segments. However, the increase of the packing fraction was fundamental to observe other kinds of alignment as, e.g., parallel and antiparallel arrangements of the dipoles. Given the preference of head-to-tail configurations and thus chain formation, we paid special attention to the appearance of a cluster extending over the whole system for sufficient large packing fraction (percolated cluster). Nevertheless, the side-by-side arrangement and the two-dimensional confinement suppresses the percolation transition for higher aspect ratio. Such a behavior is opposite to what was observed in 3D [25,34]. This result should also be contrasted to an earlier study of a nonmagnetic filament network system of rods and crosslinkers in which the percolation transition was independent of the filament length [55].

The transition to the isotropic-nematic phase was facilitated by the increase of the aspect ratio of the rods. However, the nematic behavior did not exhibit any monotonic behavior with respect to the packing fraction due to the presence of magnetic bulk domains at large η values, characterized by local ferromagnetic order. Specifically, for $l = 1$, the nematic behavior in the bulk domain was followed by hexagonal order which is expected in the limit of high density and low temperature.

The results shown in this work were obtained for low temperature ($T^* = 0.1$). For temperatures one order of magnitude smaller (higher) than the one considered here, $T^* = 0.1$, the percolation transition occurs at lower (higher) values of the packing fraction, as observed in Ref. [50]. For sufficiently high temperatures the clusters are destroyed, suppressing the percolation transition. A more detailed systematic study of the temperature dependence of the structural properties of the present study is left to future work.

ACKNOWLEDGMENTS

This work was supported by the Brazilian agencies FUNCAP, CAPES, program Science without borders, and CNPq (Project No. 400748/2013-4), the joint CNPq-FWO bilateral project, and the Flemish Science Foundation (FWO-V1).

APPENDIX: TORQUE ON A MAGNETIC ROD OF SINGLE DIPOLAR BEADS

We derive the expression for the torque on a rod consisting of single dipoles. To derive Eq. (6), we must go back to the definition of the torque on a current distribution $\mathbf{J}(\mathbf{r})$. The infinitesimal torque on the volume element dV with current distribution $\mathbf{J}(\mathbf{r})$ in a nonuniform magnetic field is

$$d\mathbf{N}_{o'} = (\mathbf{r}_i - \mathbf{r}_{o'}) \times \mathbf{J} \times \mathbf{B} dV, \tag{A1}$$

where $\mathbf{r}_i$ is the position of dV (where $\mathbf{B}$ acts). The torque is calculated with respect to the point located at $\mathbf{r}_{o'}$. $\mathbf{r}_i - \mathbf{r}_{o'}$ is the displacement vector.

The problem is the contribution of the torque on each dipole moment when the point, where this property is measured, is out of the "center" of the dipole, i.e., $\mathbf{r}_{o'}$. However, the expression of torque on a dipole moment calculated with respect to its center (center of current distribution), namely $\mathbf{r}_o$, is already known. Adding and subtracting $\mathbf{r}_o \times \mathbf{J} \times \mathbf{B} dV$ to Eq. (A1):

$$d\mathbf{N}_{o'} = (\mathbf{r}_i + \mathbf{r}_o - \mathbf{r}_o - \mathbf{r}_{o'}) \times \mathbf{J} \times \mathbf{B} dV. \tag{A2}$$

Rearranging and integrating Eq. (A2) over the volume we obtain

$$\mathbf{N}_{o'} = \int_V (\mathbf{r}_i - \mathbf{r}_o) \times \mathbf{J} \times \mathbf{B} dV + (\mathbf{r}_o - \mathbf{r}_{o'}) \times \int_V \mathbf{J} \times \mathbf{B} dV. \tag{A3}$$

As the magnetic field is nonuniform, we may perform a Taylor's expansion in $\mathbf{B}(\mathbf{r})$ around a vector which localizes the coordinate of the dipole moment $\mathbf{r}_d$, as long as $\mathbf{B}(\mathbf{r})$ does not vary significantly over $\mathbf{r}_d$:

$$\mathbf{B}(\mathbf{r}) = \mathbf{B}(\mathbf{r}_d) + [(\mathbf{r} - \mathbf{r}_d) \cdot \nabla_d] \mathbf{B}(\mathbf{r}_d) + \cdots. \tag{A4}$$

Next we use [74]

$$\boldsymbol{\mu} \times \mathbf{B}(\mathbf{r}_d) = \int_V \mathbf{r} \times [\mathbf{J}(\mathbf{r}) \times \mathbf{B}(\mathbf{r}_d)] dV,$$

$$\mathbf{F} = \int_V \mathbf{J}(\mathbf{r}) \times \mathbf{B} dV,$$

where $\mathbf{F}$ is the net force on the current distribution. Finally, we find

$$\mathbf{N}_{o'} = \boldsymbol{\mu} \times \mathbf{B}(\mathbf{r}_d) + (\mathbf{r}_o - \mathbf{r}_{o'}) \times \mathbf{F}. \tag{A5}$$

In our model we use

$$\mathbf{B}(\mathbf{r}_d) = \sum_{m \neq j} \mathbf{B}_{jm}, \quad \mathbf{F} = \sum_{m \neq j} \mathbf{f}_{jm}, \quad \text{and} \quad \mathbf{r}_o - \mathbf{r}_{o'} = \mathbf{d}_o.$$

[1] T. Albrecht, C. Bührer, M. Fähnle, K. Maier, D. Platzek, and J. Reske, Appl. Phys. A **65**, 215 (1997).
[2] A. K. Gupta and M. Gupta, Biomaterials **26**, 3995 (2005).
[3] E. Duguet, S. Mornet, S. Vasseur, F. Grasset, P. Veverka, G. Goglio, A. Demourgues, J. Portier, and E. Pollert, Prog. Solid State Chem. **34**, 237 (2006).
[4] T. Hyeon, Chem. Commun. **2003**, 927 (2003).
[5] S. L. Biswal and A. P. Gast, Phys. Rev. E **68**, 021402 (2003).
[6] C. Goubault, P. Jop, M. Fermigier, J. Baudry, E. Bertrand, and J. Bibette, Phys. Rev. Lett. **91**, 260802 (2003).
[7] J. M. Dempster, P. Vazquez-Montejo, and M. Olvera de la Cruz, Phys. Rev. E **95**, 052606 (2017).
[8] S. Gubin, *Magnetic Nanoparticles* (Wiley, New York, 2009).
[9] K. J. Lee, J. Yoon, and J. Lahann, Curr. Opin. Colloid Interface Sci. **16**, 195 (2011).
[10] P. Tierno, Phys. Chem. Chem. Phys. **16**, 23515 (2014).
[11] P. Bender, A. Tschöpe, and R. Birringer, J. Magn. Magn. Mater. **346**, 152 (2013).
[12] R. Colin, L. Chevry, J. F. Berret, and B. Abou, Soft Matter **10**, 1167 (2014).
[13] T. Petit, L. Zhang, K. E. Peyer, B. E. Kratochvil, and B. J. Nelson, Nano Lett. **12**, 156 (2011).
[14] T. Sawetzki, S. Rahmouni, C. Bechinger, and D. W. Marr, Proc. Natl. Acad. Sci. USA **105**, 20141 (2008).
[15] B. Kavčič, D. Babič, N. Osterman, B. Podobnik, and I. Poberaj, Appl. Phys. Lett. **95**, 023504 (2009).
[16] C. E. Sing, L. Schmid, M. F. Schneider, T. Franke, and A. Alexander-Katz, Proc. Natl. Acad. Sci. USA **107**, 535 (2010).
[17] L. Zhang, T. Petit, Y. Lu, B. E. Kratochvil, K. E. Peyer, R. Pei, J. Lou, and B. J. Nelson, ACS Nano **4**, 6228 (2010).
[18] T. R. Kline, W. F. Paxton, T. E. Mallouk, and A. Sen, Angew. Chem. **117**, 754 (2005).
[19] B. J. Lemaire, P. Davidson, J. Ferré, J. P. Jamet, P. Panine, I. Dozov, and J. P. Jolivet, Phys. Rev. Lett. **88**, 125507 (2002).
[20] J. Philip, P. Shima, and B. Raj, Appl. Phys. Lett. **91**, 203108 (2007).
[21] Y. Piao, J. Kim, H. B. Na, D. Kim, J. S. Baek, M. K. Ko, J. H. Lee, M. Shokouhimehr, and T. Hyeon, Nat. Mater. **7**, 242 (2008).
[22] J. Yan, K. Chaudharyn, S. C. Bae, J. A. Lewis, and S. Granick, Nat. Commun. **4**, 1516 (2013).
[23] F. Martinez-Pedrero, A. Cebers, and P. Tierno, Phys. Rev. Appl. **6**, 034002 (2016).
[24] R. Birringer, H. Wolf, C. Lang, A. Tschöpe, and A. Michels, Z. Phys. Chem. **222**, 229 (2008).
[25] C. E. Alvarez and S. H. Klapp, Soft Matter **8**, 7480 (2012).
[26] J. L. Baker, A. Widmer-Cooper, M. F. Toney, P. L. Geissler, and A. P. Alivisatos, Nano Lett. **10**, 195 (2009).
[27] K. H. Bhatt and O. D. Velev, Langmuir **20**, 467 (2004).
[28] N. Osterman, D. Babič, I. Poberaj, J. Dobnikar, and P. Ziherl, Phys. Rev. Lett. **99**, 248301 (2007).
[29] J. J. Juàrez and M. A. Bevan, J. Chem. Phys. **131**, 134704 (2009).
[30] O. D. Velev and S. Gupta, Adv. Mater. **21**, 1897 (2009).
[31] G. Zarragoicoechea, D. Levesque, and J. Weis, Mol. Phys. **75**, 989 (1992).
[32] S. C. McGrother, A. Gil-Villegas, and G. Jackson, Mol. Phys. **95**, 657 (1998).
[33] J. Philip, P. Shima, and B. Raj, Appl. Phys. Lett. **92**, 043108 (2008).

[34] K. Leung and D. Chandler, J. Stat. Phys. **63**, 837 (1991).
[35] T. Schilling, S. Jungblut, and M. A. Miller, Phys. Rev. Lett. **98**, 108303 (2007).
[36] R. H. J. Otten and P. van der Schoot, Phys. Rev. Lett. **108**, 088301 (2012).
[37] R. F. Kayser and H. J. Raveché, Phys. Rev. A **17**, 2067 (1978).
[38] M. E. van Leeuwen and B. Smit, Phys. Rev. Lett. **71**, 3991 (1993).
[39] B. Groh and S. Dietrich, Phys. Rev. E **50**, 3814 (1994).
[40] H. J. Berendsen, J. P. M. Postma, W. F. van Gunsteren, A. DiNola, and J. Haak, J. Chem. Phys. **81**, 3684 (1984).
[41] We are aware that the Berendsen thermostat does not include the temperature fluctuations in the canonical ensemble [42]. We also performed Langevin dynamics and microcanonical MD simulations and the results are consistent with those obtained with the Berendsen thermostat, which led us to conclude that the physical properties studied in the present work are not sensitive to the choice of the thermostat.
[42] I. Solov'yov, A. Yakubovich, P. Nikolaev, I. Volkovets, and A. Solov'yov, J. Comput. Chem. **33**, 2412 (2012).
[43] M. P. Allen and D. J. Tildesley, *Computer Simulation of Liquids* (Oxford University Press, Oxford, 1989).
[44] G. De Las Cuevas, J. Faraudo, and J. Camacho, J. Phys. Chem. C **112**, 945 (2008).
[45] J. Weis, Mol. Phys. **93**, 361 (1998).
[46] R. Chantrell, A. Bradbury, J. Popplewell, and S. Charles, J. Appl. Phys. **53**, 2742 (1982).
[47] J. M. Tavares, J. J. Weis, and M. M. Teloda Gama, Phys. Rev. E **65**, 061201 (2002).
[48] K. Butter, P. Bomans, P. Frederik, G. Vroege, and A. Philipse, Nat. Mater. **2**, 88 (2003).
[49] S. S. Das, A. P. Andrews, and S. Greer, J. Chem. Phys. **102**, 2951 (1995).
[50] H. Schmidle, C. K. Hall, O. D. Velev, and S. H. Klapp, Soft Matter **8**, 1521 (2012).
[51] D. C. Rapaport, *The Art of Molecular Dynamics Simulation* (Cambridge University Press, Cambridge, 2004).
[52] D. Stauffer and A. Aharony, *Introduction to Percolation Theory* (Taylor Francis Group, London, 1994).
[53] M. A. Miller, R. Blaak, C. N. Lumb, and J.-P. Hansen, J. Chem. Phys. **130**, 114507 (2009).
[54] Y. Liu and R. Pandey, J. Chem. Phys. **105**, 825 (1996).
[55] R. Chelakkot and T. Gruhn, Soft Matter **8**, 11746 (2012).
[56] M. T. A. Bos and J. H. J. van Opheusden, Phys. Rev. E **53**, 5044 (1996).
[57] M. Rubinstein and R. H. Colby, *Polymer Physics* (Oxford University Press, Oxford, 2003).
[58] L. V. Woodcock, AIChE J. **58**, 1610 (2012).
[59] P. D. Godfrin, N. E. Valadez-Pérez, R. Castaneda-Priego, N. J. Wagner, and Y. Liu, Soft Matter **10**, 5061 (2014).
[60] G. E. Pike and C. H. Seager, Phys. Rev. B **10**, 1421 (1974).
[61] A. L. R. Bug, S. A. Safran, and I. Webman, Phys. Rev. Lett. **54**, 1412 (1985).
[62] F. Sciortino, P. Tartaglia, and E. Zaccarelli, J. Phys. Chem. B **109**, 21942 (2005).
[63] J. Weis, Mol. Phys. **100**, 579 (2002).
[64] D. R. Nelson and R. A. Pelcovits, Phys. Rev. B **16**, 2191 (1977).
[65] J. Toner and D. R. Nelson, Phys. Rev. B **23**, 316 (1981).
[66] M. A. Bates and D. Frenkel, J. Chem. Phys. **112**, 10034 (2000).
[67] R. Tavarone, P. Charbonneau, and H. Stark, J. Chem. Phys. **143**, 114505 (2015).
[68] M. Abkenar, K. Marx, T. Auth, and G. Gompper, Phys. Rev. E **88**, 062314 (2013).
[69] T. Geigenfeind, S. Rosenzweig, M. Schmidt, and D. de las Heras, J. Chem. Phys. **142**, 174701 (2015).
[70] J. Dzubiella, G. P. Hoffmann, and H. Löwen, Phys. Rev. E **65**, 021402 (2002).
[71] H. Lowen, Soft Matter **6**, 3133 (2010).
[72] F. Ginelli, F. Peruani, M. Bär, and H. Chaté, Phys. Rev. Lett. **104**, 184502 (2010).
[73] S. R. McCandlish, A. Baskaran, and M. F. Hagan, Soft Matter **8**, 2527 (2012).
[74] K. D. Machado, *Teoria do Eletromagnetismo* (UEPG, Ponta Grossa, 2002), Vol. 2.